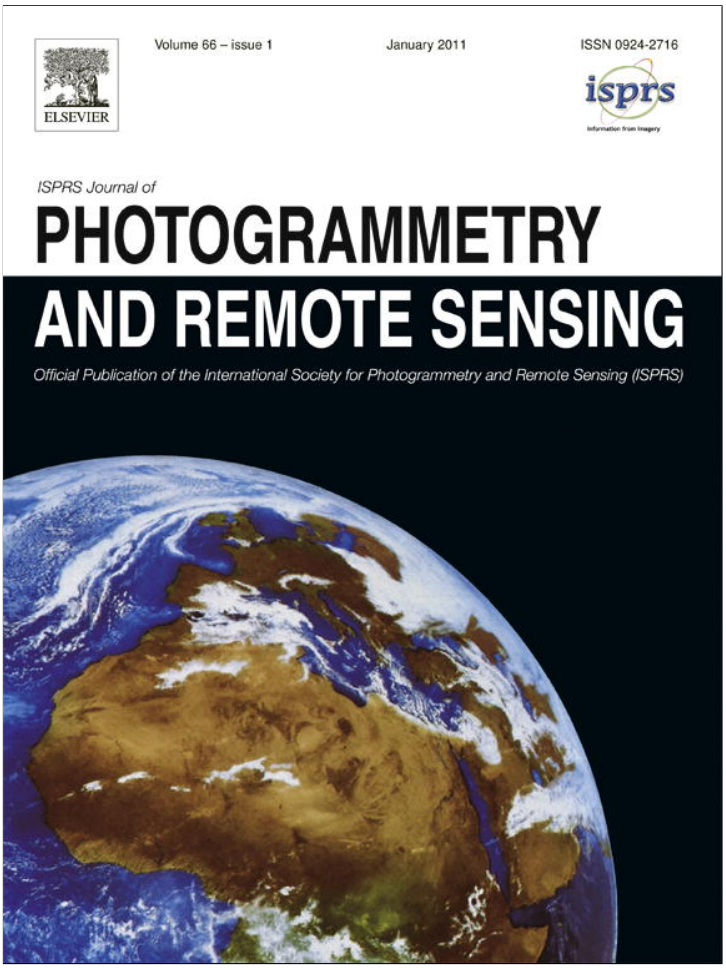

(This is a sample cover image for this issue. The actual cover is not yet available at this time.)

ISPRS Journal of Photogrammetry and Remote Sensing 66 (2011) 798–808

Contents lists available at SciVerse ScienceDirect

ISPRS Journal of Photogrammetry and Remote Sensing

journal homepage: www.elsevier.com/locate/isprsjprs

Mapping impervious surfaces with the integrated use of Landsat Thematic Mapper and radar data: A case study in an urban–rural landscape in the Brazilian Amazon

Dengsheng Lu [a,*], Guiying Li [a,1], Emilio Moran [a,1], Mateus Batistella [b,2], Corina C. Freitas [c,3]

[a] Anthropological Center for Training and Research on Global Environmental Change (ACT), Indiana University, Bloomington, IN 47405, USA
[b] Embrapa Satellite Monitoring, Av. Julio Soares de Arruda, 803, Campinas, SP 13088-300, Brazil
[c] National Institute for Space Research, Av. dos Astronautas, 1758, São Jose dos Campos, SP 12245-010, Brazil

ARTICLE INFO

Article history:
Received 31 March 2011
Received in revised form 22 July 2011
Accepted 15 August 2011

Keywords:
Landsat TM
ALOS PALSAR L-band
RADARSAT-2 C-band
Wavelet-merging technique
Spectral mixture analysis
Impervious surface

ABSTRACT

This research explored the integrated use of Landsat Thematic Mapper (TM) and radar (i.e., ALOS PALSAR L-band and RADARSAT-2 C-band) data for mapping impervious surface distribution to examine the roles of radar data with different spatial resolutions and wavelengths. The wavelet-merging technique was used to merge TM and radar data to generate a new dataset. A constrained least-squares solution was used to unmix TM multispectral data and multisensor fusion images to four fraction images (high-albedo, low-albedo, vegetation, and soil). The impervious surface image was then extracted from the high-albedo and low-albedo fraction images. QuickBird imagery was used to develop an impervious surface image for use as reference data to evaluate the results from TM and fusion images. This research indicated that increasing spatial resolution by multisensor fusion improved spatial patterns of impervious surface distribution, but cannot significantly improve the statistical area accuracy. This research also indicated that the fusion image with 10-m spatial resolution was suitable for mapping impervious surface spatial distribution, but TM multispectral image with 30 m was too coarse in a complex urban–rural landscape. On the other hand, this research showed that no significant difference in improving impervious surface mapping performance by using either PALSAR L-band or RADARSAT C-band data with the same spatial resolution when they were used for multi-sensor fusion with the wavelet-based method.

1. Introduction

The colonization projects initiated in the 1970s have resulted in a large area conversion from primary forest and cerrado/savanna to agriculture, pasture, agroforestry, and secondary succession in the Brazilian Amazon (Lucas et al., 2000; Roberts et al., 2002; Ferreira et al., 2004; Sano et al., 2010). As people have migrated from different parts of Brazil to the Amazon over the last several decades, road construction and urban expansion rates have rapidly increased, thus mapping urban land cover in the Amazon has received growing attention (Powell et al., 2007; Powell and Roberts, 2008, 2010). Because of the complex urban landscape, directly mapping urban distribution with remotely sensed data is often difficult (Lu and Weng, 2004). Impervious surface area has been regarded as a critical variable for examining urban expansion. Therefore, mapping impervious surfaces with satellite images has received considerable attention in the past decade (Wu and Murray, 2003; Yang et al., 2003, 2010; Lu and Weng, 2006; Xian et al., 2008; Weng et al., 2009; Lu et al., 2011b). Slonecker et al. (2001) reviewed three basic approaches for impervious surface extraction from remotely sensed data based on the achievements in the 1970s and 1980s. Brabec et al. (2002) summarized four categories of methods for impervious surface mapping. Many advanced algorithms have been developed for quantitative extraction of impervious surfaces from satellite imagery in the past decade and they are summarized in Lu et al. (in press).

In urban environments, land covers can be regarded as a linear combination of three components: vegetation, impervious surface, and soil (V–I–S) (Ridd, 1995). The V–I–S model provides a guideline for decomposing urban landscapes and a linkage for these components to remote-sensing spectral characteristics. In reality, impervious surfaces are very complex land covers that consist of

* Corresponding author. Tel.: +1 812 855 6182; fax: +1 812 855 3000.
E-mail addresses: dlu@indiana.edu (D. Lu), ligu@indiana.edu (G. Li), moran@zindiana.edu (E. Moran), mb@cnpm.embrapa.br (M. Batistella), corina@dpi.inpe.br (C.C. Freitas).
[1] Tel.: +1 812 855 6182; fax: +1 812 855 3000.
[2] Tel.: +55 19 3256 6030.
[3] Tel.: +55 12 3208 6000.

0924-2716/$ - see front matter © 2011 International Society for Photogrammetry and Remote Sensing, Inc. (ISPRS). Published by Elsevier B.V. All rights reserved.
doi:10.1016/j.isprsjprs.2011.08.004

different structures, colors, and materials, thus manifest high spectral variation in remotely sensed data. For example, some building roofs have very high spectral values that are confused with bare soils, and some dark roads/streets have very low spectral values that are often confused with water/wetland/shadow (Lu et al., 2011b). Because of this special characteristic of impervious surfaces, direct extraction of impervious surfaces from remotely sensed data based on spectral signatures is very difficult (Lu and Weng, 2004). We can assume that an urban landscape is composed of four fraction components—high-albedo object ($f_{high\text{-}albedo}$), low-albedo object ($f_{low\text{-}albedo}$), green vegetation (f_{GV}), and soil (f_{Soil})—because land covers consist of these four components, with either a linear or nonlinear relationship. High-albedo object represents the land covers with high spectral reflectance, such as bright impervious surfaces and dry bare soils; low-albedo object represents the land covers with low spectral reflectance, such as dark impervious surfaces, forested shade, water and wetland (Lu and Weng, 2006). Previous research has indicated that these four fractions can be developed with spectral mixture analysis (Wu and Murray, 2003; Lu and Weng, 2006). Since impervious surfaces are mainly concentrated on the high- and low-albedo fraction images, they can be extracted from the addition of high- and low-albedo fraction images after removal of the non-impervious surface pixels through established rules (Lu and Weng, 2006; Lu et al., 2011b).

Most previous research on impervious surface mapping was based on Landsat images, but the spatial resolution of 30 m was often regarded as too coarse for mapping urban biophysical descriptors (Jensen and Cowen, 1999), especially in the complex urban–rural landscape in the Brazilian Amazon (Lu et al., 2011b). In recent decades, high spatial resolution satellite images such as QuickBird, IKONOS, and WorldView have been available and used in many applications, such as mapping urban impervious surfaces and vegetation in relatively small areas (Goetz et al., 2003; Wang et al., 2004; Mallinis et al., 2008; Lu et al., 2011a), but they are not extensively applied to a large area due to lack of data availability and cost, as well as time and labor required to process the large volume of data. Other disadvantages of using high spatial resolution images are their high spectral variation within the same land cover, their spectral confusion between impervious surfaces and other land covers, and the shadow problems caused by tall objects, all of which present a challenge for automatically mapping impervious surface distribution (Dare, 2005; Zhou et al., 2009; Lu et al., 2011a). Therefore, a medium spatial resolution image like Landsat is still the most common data source for mapping urban impervious surfaces in a large area (Wu and Murray, 2003; Lu and Weng, 2006; Lu et al., 2011b).

In order to reduce the mixed-pixel problem, an alternative is to conduct data fusion through the incorporation of higher spatial resolution information into the multispectral image. In particular, the integration of multisensor data (e.g., TM and radar) has attracted growing attention due to their distinct information features (Lu et al., 2007; McNairn et al., 2009; Amarsaikhan et al., 2010). However, rare research has examined the combination of radar and optical sensor data in improving impervious surface mapping (Gamba and Dell'Acqua, 2008; Yang et al., 2009), especially through data fusion methods. It is poorly understood how different spatial resolutions and wavelengths of radar data affect impervious surface mapping performance. Therefore, the objective of this research is to explore the role of data fusion of Landsat and radar data in and the effect of different data spatial resolutions on improving impervious surface mapping. A Landsat TM image, ALOS PALSAR L-band and RADARSAT-2 C-band data, and a QuickBird image were selected for a complex urban–rural landscape in a moist tropical region of

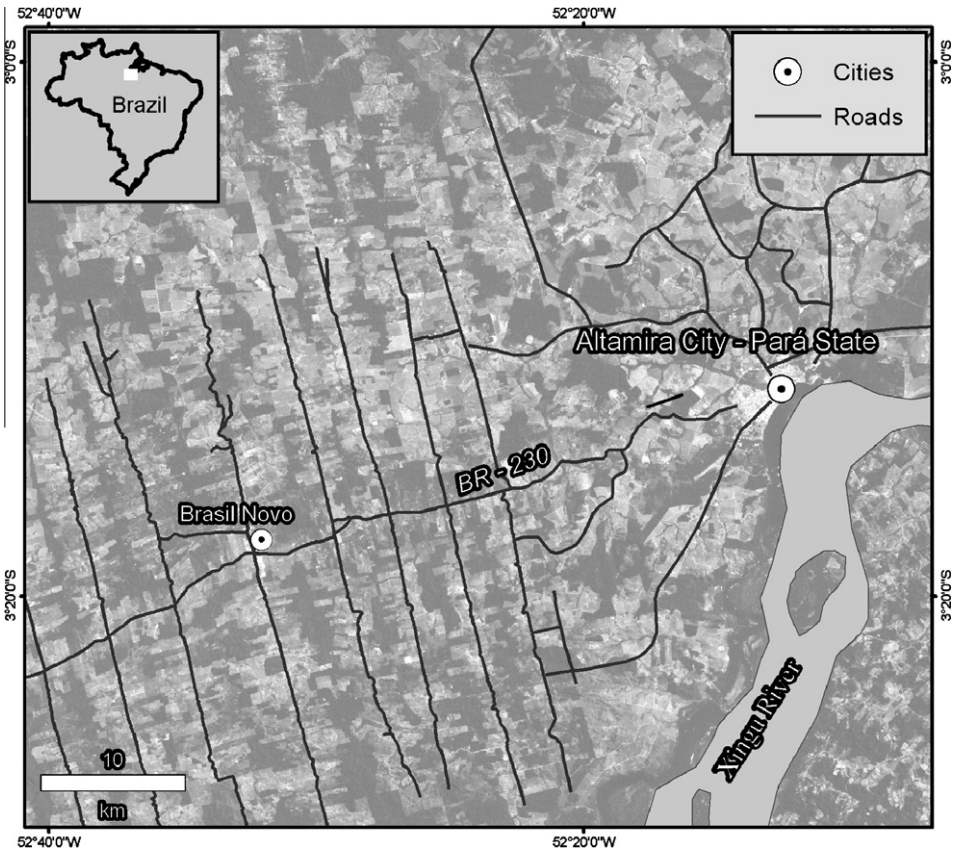

Fig. 1. Study area – Altamira, Pará State, Brazil.

the Brazilian Amazon. Spectral mixture analysis was used to map impervious surface distribution, and the results were evaluated with the QuickBird-derived impervious surface data.

2. Study area

Altamira, Brazil, has had a long history as a riverine settlement on the first big bend of the Xingú River (Fig. 1) (Moran, 1981). For most of its history it was a small trading settlement in the rubber export network during good times, and a typical, small Amazon town based on subsistence and extraction of forest products the rest of the time. That changed in 1970 when construction of the Transamazon Highway (BR-230) and its associated settlement scheme began (Moran, 1975; Smith, 1982). From the early 1970s, the region grew in population from 1000 to 50,145 in 1991, 62,285 in 2000, and 90,068 in 2010 (http://www.citypopulation.de/Brazil-Para.html). Agropastoral production has served as its mainstay. The study area covers approximately 143 km^2. Annual rainfall in Altamira is approximately 2000 mm and is concentrated from late October through early June; the dry period occurs between June and September. Average annual temperature is about 26 °C.

3. Methods

The linear spectral mixture analysis (LSMA)-based method was used to map impervious surface distribution based on different datasets—Landsat TM multispectral image and fusion images with TM and different radar data (ALOS PALSAR L-band, RADARSAT-2 C-band). A QuickBird-derived impervious surface image was used as reference data to evaluate the impervious surface results from TM and fusion images. Fig. 2 illustrates the strategy of the integration of TM and radar data for impervious surface mapping used in this research.

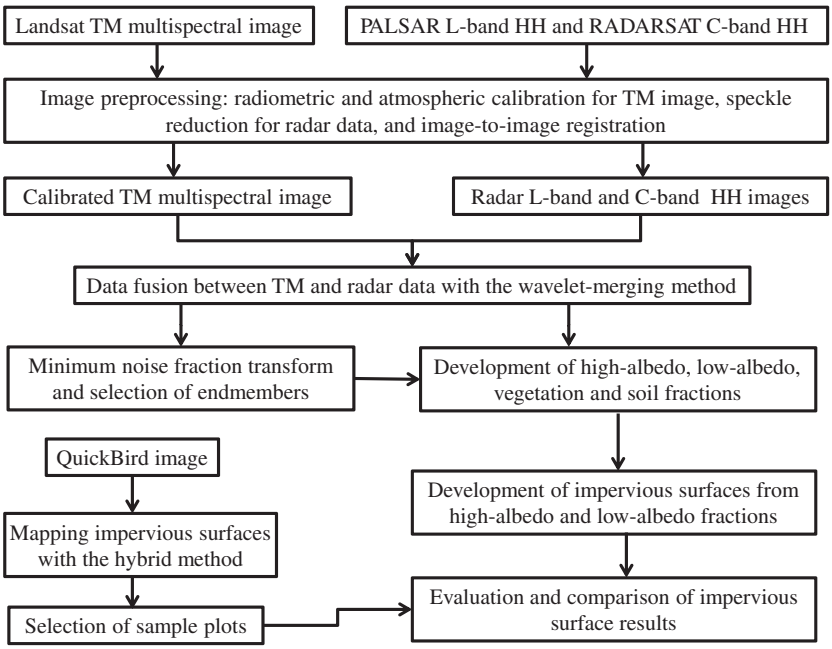

Fig. 2. Strategy of impervious surface mapping with the integration of Landsat TM and radar data.

Table 1
Satellite images used in this research.

Satellite sensors	Image acquisition date and major characteristics of datasets	Spatial resolution after image registration
Landsat 5 TM	Path/Row: 226/62 Acquired on July 2, 2008 Six multispectral bands covering visible, near-infrared and short-wave infrared wavelengths with 30-m spatial resolution	Six multispectral bands with 30-m spatial resolution
ALOS PALSAR	Acquired on July 2, 2009 L-band HH and HV with 12.5-m pixel spacing	Use only HH image, resampled to 10-m cell size
RADARSAT-2	August 16, 2009, C-band HH and HV with 3.7-m pixel spacing (SGX) August 30, 2009, C-band HH and HV with 8-m pixel spacing (SGX) August 23, 2009, C-band HH and HV with 30-m pixel spacing (SGF)	Use only HH image, resampled to 3-m cell size Use only HH image, resampled to 10-m cell size Use only HH image, resampled to 30-m cell size
QuickBird	September 26, 2008, four multispectral bands with 2.4-m and one panchromatic band with 0.6-m spatial resolution	Four bands with 1-m spatial resolution after data fusion with High Pass Filter resolution-merging method

3.1. Image collection and preprocessing

Several sensor data—Landsat TM, ALOS PALSAR L-band, RADARSAT-2 C-band, and QuickBird—were used in this research (Table 1). The TM image was geometrically registered to a previously corrected Landsat 5 TM image with UTM projection (zone 22 south). The geometric error was less than 0.5 pixels. During image-to-image registration, the nearest-neighbor resampling algorithm was used to resample the TM imagery to avoid the change of digital numbers and keep the same pixel size of 30 m by 30 m as the original image. An improved image-based dark-object subtraction model was used to perform radiometric and atmospheric correction (Chavez, 1996; Chander et al., 2009). The gain and offset for each band and sun elevation angle were obtained from the image header file. The path radiance for each band was identified from deep water bodies.

ALOS PALSAR and RADARSAT-2 are active microwave sensors using L-band and C-band frequencies, respectively, to achieve cloud-free land observation (Rosenqvist et al., 2007). In this research, the ALOS PALSAR FBD (Fine Beam Double Polarization)

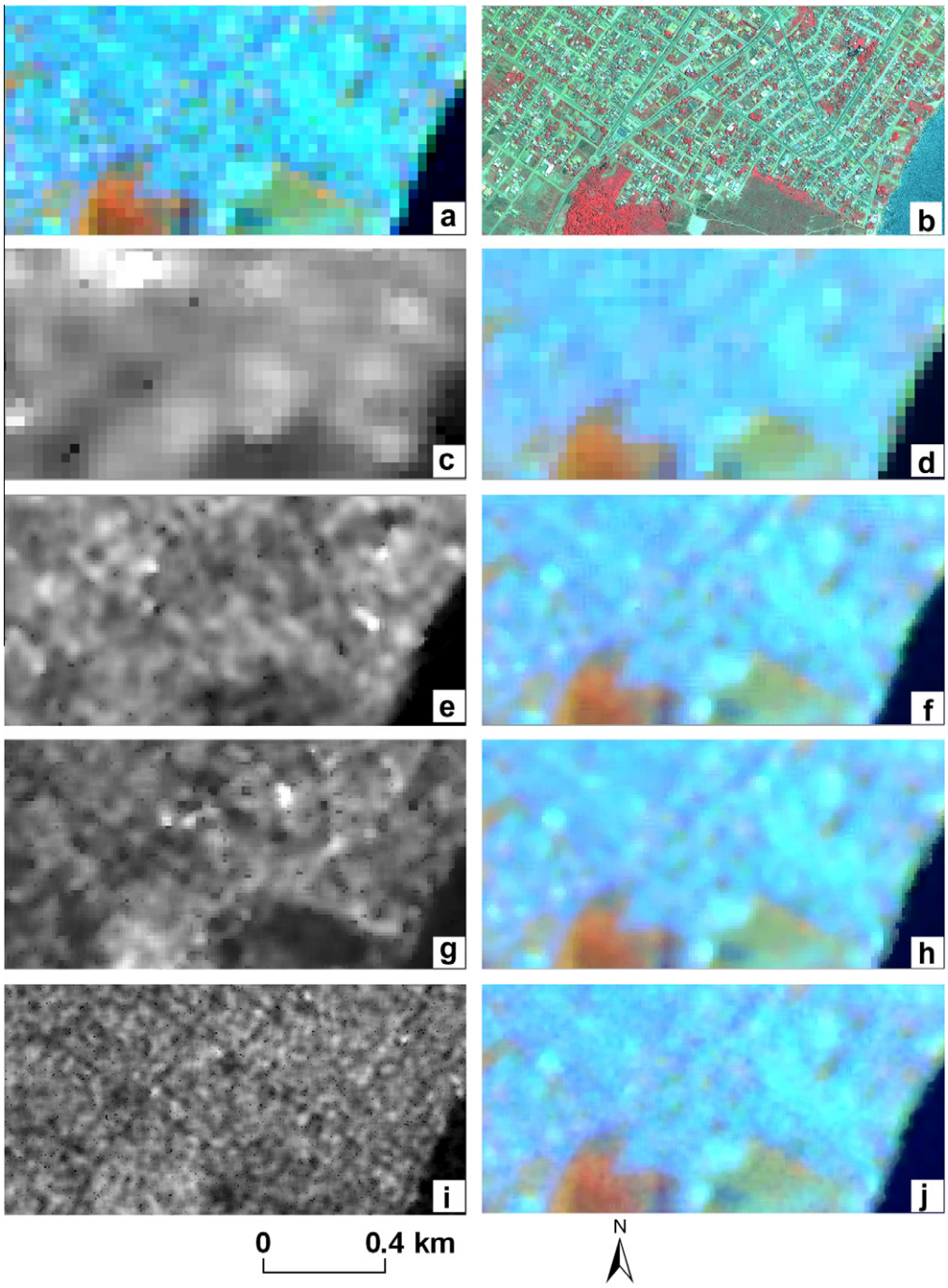

Fig. 3. A comparison of images among before- and after-data fusion with different radar data (a – color composite of TM bands 4, 5, and 3 as red, green and blue; b – QuickBird bands 4,3,2 color composite; c and e – RADARSAT-2 C-band HH image with 30 m and 10 m spatial resolutions; d and f – color composites with bands 4, 5, and 3 based on wavelet-merging fusion of TM and C-band HH 30 m and of TM and C-band HH 10 m; g – ALOS PALSAR L-band HH with 10 m spatial resolution; h – color composite with bands 4, 5, and 3 based on wavelet-merging fusion of TM and L-band HH 10 m; i – RADARSAT-2 C-band HH image with 3 m spatial resolution; and j – color composite with bands 4, 5, and 3 based on wavelet-merging fusion of TM and C-band HH 3 m).

Level 1.5 products with HH (the radiation was horizontally polarized and the antenna only received horizontally polarized radiation) and HV (the transmitted radiation was vertically polarized and the polarization of the received radiation was restricted to just horizontally polarized waves) polarization options (ground range, unsigned 16-bit integral number, 12.5-m pixel spacing) (ESA, 2007) and RADARSAT-2 C-band, also with HH and HV polarization options, as well as different pixel sizes were used (Table 1). Based on our previous research (Lu et al., 2011c), the Lee-Sigma filtering method with a 5×5 window was selected for this research to reduce the speckle problem. Both radar L-band and C-band images were registered into UTM projection. The PALSAR L-band images with original 12.5-m pixel spacing and RADARSAT-2 C-band with original 8-m pixel spacing were registered to a previously rectified ASTER image, and both were resampled to 10-m cell size with the nearest-neighbor resampling algorithm. The RADARSAT-2 C-band image with original 3.7-m pixel spacing was registered to a QuickBird image and resampled to 3-m cell size, and the RADARSAT-2 C-band image with original 30-m pixel spacing was registered to a previously rectified ASTER image. The geometric errors, i.e., root-mean square errors, for all radar data were less than 30 m (less than one pixel in TM image) for the image-to-image registration.

3.2. Data fusion of Landsat TM and radar data

Data fusion is often used for the integration of multisensor or multiresolution data to enhance visual interpretation and/or to improve quantitative analysis performance. Many data fusion methods, such as principal component analysis (PCA), wavelet-merging technique, intensity-hue-saturation (IHS), Brovey transform, color normalization spectral sharpening, Gram Schmidt fusion, and Ehlers fusion have been applied to integrate spectral and spatial information (Dai and Khorram, 1998; Pohl and van Genderen, 1998; Chen and Stow, 2003; Ulfarsson et al., 2003; Zhang, 2004,2010; Dong et al., 2009; Amarsaikhan et al., 2010; Ehlers et al., 2010). In particular, the wavelet-merging technique is regarded as a good method for preserving the multispectral features while improving the spatial features in the output (Ulfarsson et al., 2003; Amolins et al., 2007; Hong and Zhang, 2008; Lu et al., 2011c).

Lu et al. (2011c) have detailed the wavelet-merging techniques and explored the roles of different polarization options (HH and HV) from both PALSAR L-band and RADARSAT-2 C-band data for improving land-cover classification in this study area. Since our previous research indicated that the data fusion results from using radar HH data perform similarly in land-cover classification compared to results from using radar HV data (Lu et al., 2011c), this research used only radar HH imagery for data fusion. Thus, this research used ALOS PALSAR L-band HH image with 10-m pixel size and RADARSAT-2 C-band HH images with 30-m, 10-m, and 3-m pixel sizes, and then generated fusion results from Landsat TM multispectral bands and radar data with different pixel sizes. Because of the noise in the fusion images, a median filtering method based on a window size of 3×3 pixels was used on the fusion images.

3.3. Impervious surface mapping with spectral mixture analysis method

Of the many methods for mapping impervious surfaces (Slonecker et al., 2001; Brabec et al., 2002; Yang et al., 2010; Lu et al., in press), the LSMA method has proven valuable for extracting fractional impervious surfaces from Landsat images (Wu and Murray, 2003; Lu and Weng, 2006; Lu et al., 2011b). Since much previous literature (e.g., Smith et al., 1990; Adams et al., 1995; Mustard and Sunshine, 1999) has described the LSMA method, it is not detailed here.

In this research, minimum noise fraction (MNF) transform was used to convert TM multispectral bands or fusion images into a new dataset in which the majority of original information was concentrated in the first three or four components. The first three components were then used to identify four end members (i.e., high-albedo objects, low-albedo objects, vegetation, and soil), as much previous literature described (e.g., Lu and Weng, 2004, 2006). A constrained least-squares solution was then used to unmix the Landsat TM image or fusion images into four fractional images. Because the majority of bright impervious surfaces are concentrated on the $f_{high\text{-}albedo}$ image, and dark impervious surfaces are concentrated on the $f_{low\text{-}albedo}$ image, the overall impervious surface is the sum of $f_{high\text{-}albedo}$ and $f_{low\text{-}albedo}$ images (Lu and Weng, 2006). The complexity of impervious surfaces and their confusion with other land covers often generate data in which some bare soils are included in the $f_{high\text{-}albedo}$ image, and water/wetland are included in the $f_{low\text{-}albedo}$ image. It is important to remove these non-impervious surface pixels on $f_{high\text{-}albedo}$ and $f_{low\text{-}albedo}$ images. We can overlay the individual fraction image on the TM color composite, displaying the histogram of the fraction image and interactively testing different threshold values in order to identify an optimal threshold to separate the class of interest from other land covers. For example, we found that agricultural lands and some degraded pastures have f_{Soil} value of greater than 0.5; thus, we can use a threshold of 0.5 to remove the pixels with high soil fraction values in the high-albedo fraction image. Based on the analysis of major land covers (vegetation, bare soils in agricultural lands, and water/wetland) on the fraction images, the following conditions were used to remove non-impervious surface pixels: if a pixel value in a fraction image meets $f_{Soil} > 0.5$ (remove bare soils) or $f_{GV} > 0.5$ (remove vegetation) or $f_{low\text{-}albedo} > 0.99$ (remove water) or $f_{high\text{-}albedo} < 0.05$ (remove other potential non-impervious

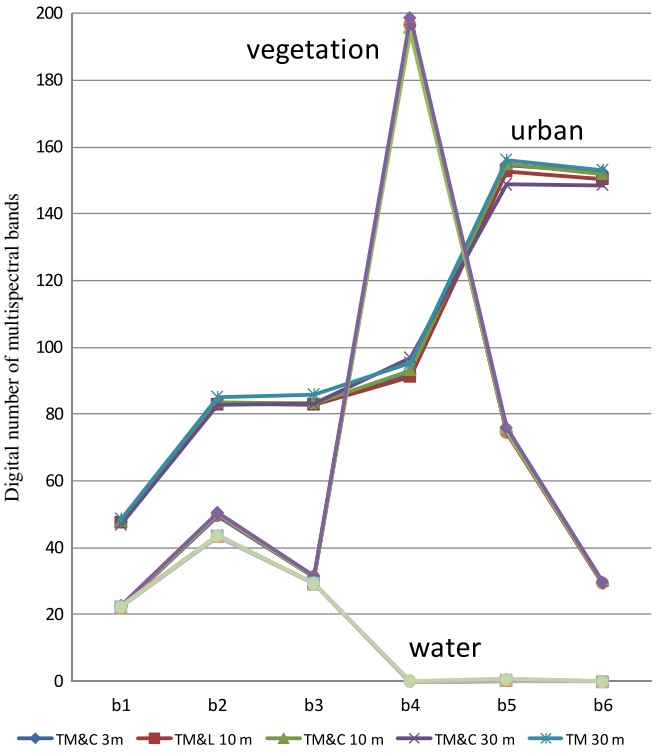

Fig. 4. Comparison of spectral signatures among data fusion results as well as TM image.

surface areas), this pixel is assigned as non-impervious surfaces; otherwise, the pixel is assigned as impervious surfaces.

3.4. Evaluation of impervious surface results

Selection of a sufficient number of sample plots with suitable resampling technique is critical for evaluation of impervious surface results. Because impervious surfaces from Landsat TM or fusion images are fractional values, traditional accuracy assessment methods (Congalton and Green, 2008) based on per-pixel level is obviously not suitable. Therefore, this research used root mean square error (RMSE), residual analysis, and correlation analysis (Lu and Weng, 2006) to evaluate the impervious surface results from TM and fusion images. In order to obtain fractional impervious surface reference data, a QuickBird image was used to develop the impervious surface image based on a previously developed method—a hybrid method consisting of thresholding, unsupervised classification and manual editing (Lu et al., 2011a). The major steps for the hybrid approach include: (1) producing the NDVI (Normalized Difference Vegetation Index) image from QuickBird red and near-infrared (NIR) images and then masking vegetation out with the selected threshold on the NDVI image; and masking

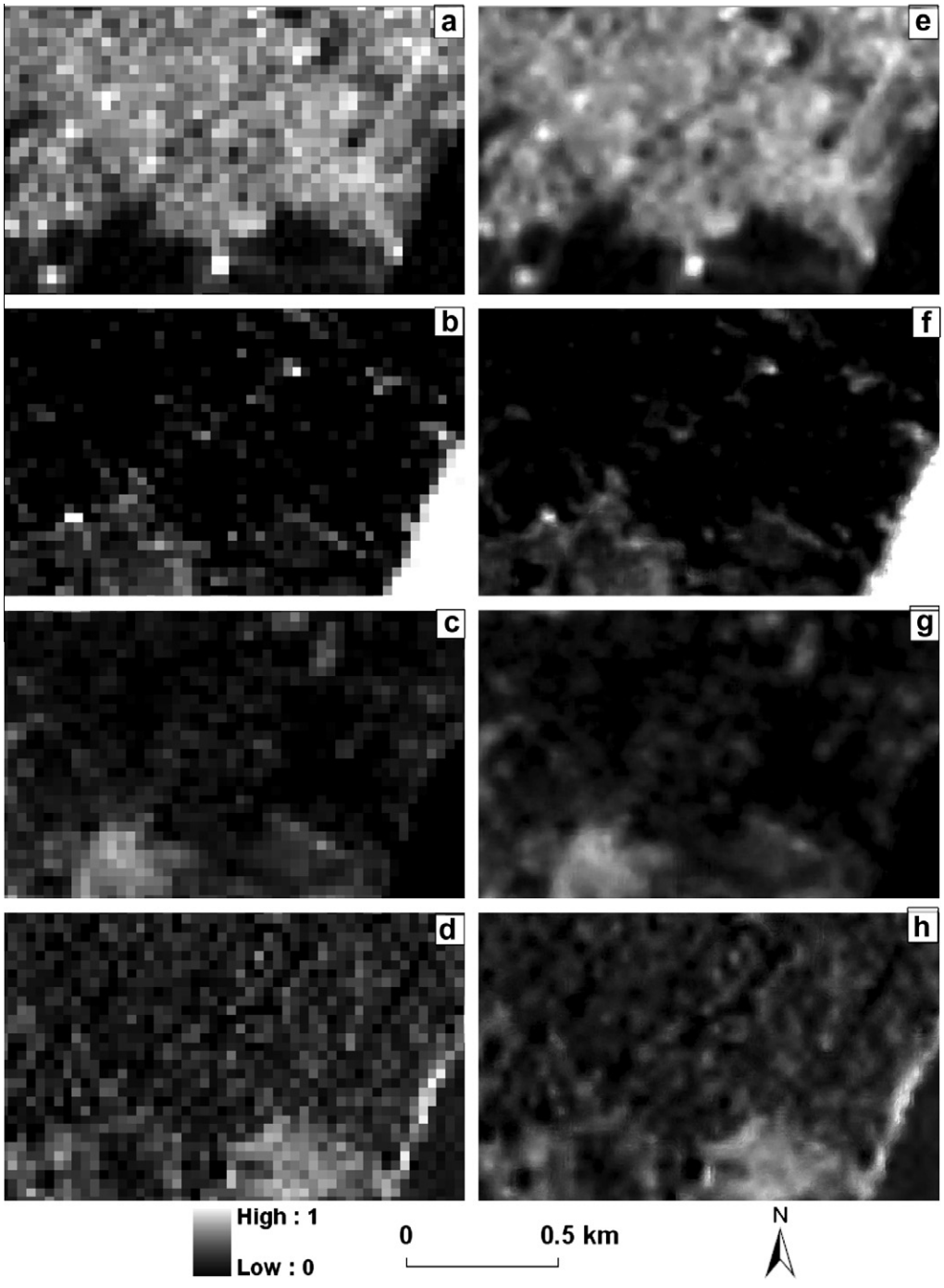

Fig. 5. A comparison of fraction images with different spatial resolutions (a,b,c,d – high-albedo, low-albedo, green vegetation, and soil fractions developed from Landsat TM multispectral image with 30 m spatial resolution; e,f,g,h – high-albedo, low-albedo, green vegetation, and soil fractions developed from the data fusion image with 3 m spatial resolution based on TM and RADARSAT-2 C-band HH image with 3 m).

water out with the threshold on the NIR image; (2) extracting spectral signatures of the non-vegetation pixels, and using an unsupervised classification algorithm to classify the extracted spectral signatures into 50 clusters. The analyst is responsible for merging the clusters into impervious surface and other classes; (3) manually editing the extracted impervious surface image to eliminate the non-impervious surfaces such as bare soils, shadows, and wetlands which have been included with the impervious surface class due to spectral confusion. The hybrid method had been used in Santarém, Para State and Lucas do Rio Verde, Mato Grosso State, Brazil, and over 98% of overall accuracy for both study areas were obtained (Lu et al., 2011a).

A total of 250 points were randomly selected based on the QuickBird-derived impervious surface image in this study area. Each point location was used as a center and a square with sizes of 30 × 30 m and 90 × 90 m (i.e., corresponding to one pixel and a window size of 3 × 3 pixels on a Landsat TM image) were created using the GIS technique. The polygons located in clouds, shadows, and outside the boundary of the QuickBird image were removed. Thus, a total of 215 polygons were used for the evaluation of impervious surface results. The mean impervious surface value for each polygon based on selected window sizes of 30 × 30 m and 90 × 90 m were calculated from the QuickBird-derived impervious surface image, and the selected samples were used as reference data for evaluating the impervious surface results from Landsat-derived and multisensory fusion images. RMSE, residual analysis and regression analysis were then used to evaluate the results.

4. Resultant analysis

4.1. Analysis of data fusion images

One important objective of data fusion is to improve spatial resolution while preserving multispectral features if the fusion result is used for quantitative analysis. Fig. 3 shows part of the study area for a comparison of the data fusion results based on TM and radar data with different cell sizes. It indicates that the wavelet-merging technique can accurately preserve multispectral features while improving spatial patterns, no matter which spatial resolutions

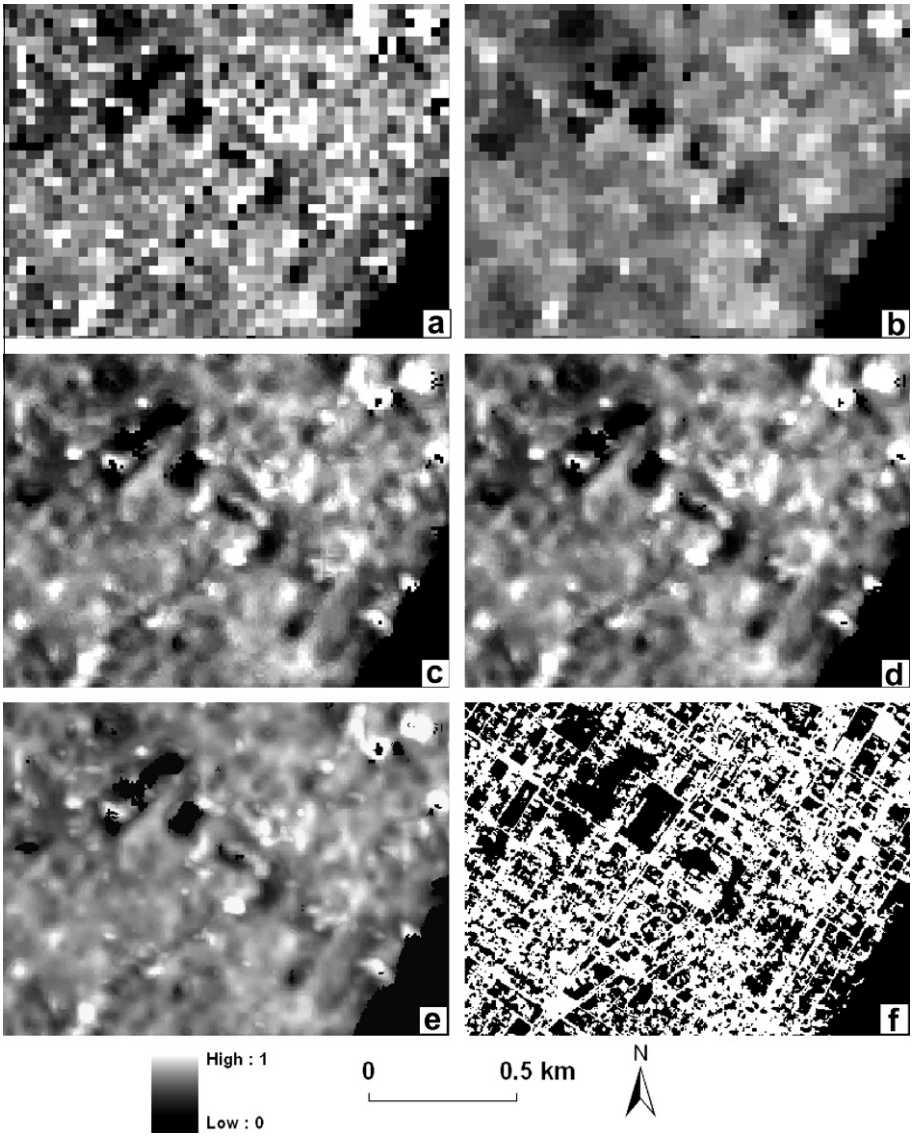

Fig. 6. A comparison of impervious surface results with different spatial resolutions (a – from TM imagery with 30 m; b – from data fusion of TM and C-band HH data with 30 m; c – from data fusion of TM and C-band HH data with 10 m; d – from data fusion of TM and L-band HH data with 10 m; e – from data fusion of TM and C-band HH data with 3 m; and f – from QuickBird image with 1 m).

(from 3 to 30 m here) and which wavelengths (L-band or C-band here) of radar data are used. In order to quantitatively compare the spectral features between before- and after-data fusion images, some land covers (e.g., forest, urban, and water) were selected on the TM image and on the fusion images, and their spectral features are illustrated in Fig. 4. This figure indicates that the fusion images preserve almost the same spectral features for vegetation and water compared to the before- and after-data fusion (the lines are overlapped), but for urban area, spectral signatures vary among the different data fusion results. This variation is due to the mixed pixels in the urban area and different radiometric information from different cell sizes of the radar images (PALSAR L-band HH image with 10-m cell size, RADARSAT-2 C-band HH images with cell sizes of 3, 10, and 30 m) incorporated into the new datasets by data fusion. This situation implies the incorporation of some radar information into the fusion image in addition to improving spatial resolution.

4.2. Comparison of impervious surface images

Previous research has indicated that impervious surfaces are mainly concentrated on the high-albedo and low-albedo fraction images (Lu and Weng, 2006; Lu et al., 2011b), as confirmed in Fig. 5. The majority of impervious surfaces are located in the high-albedo fraction image, but some dark impervious surfaces such as streets and dark building roofs are included in the low-albedo fraction image. A comparison of fraction images from Landsat TM with 30-m spatial resolution and from the fusion image based on TM and RADARSAT-2 C-band HH image with 3-m pixel spacing (Fig. 5) indicates the reduction of mixed pixel problem in the

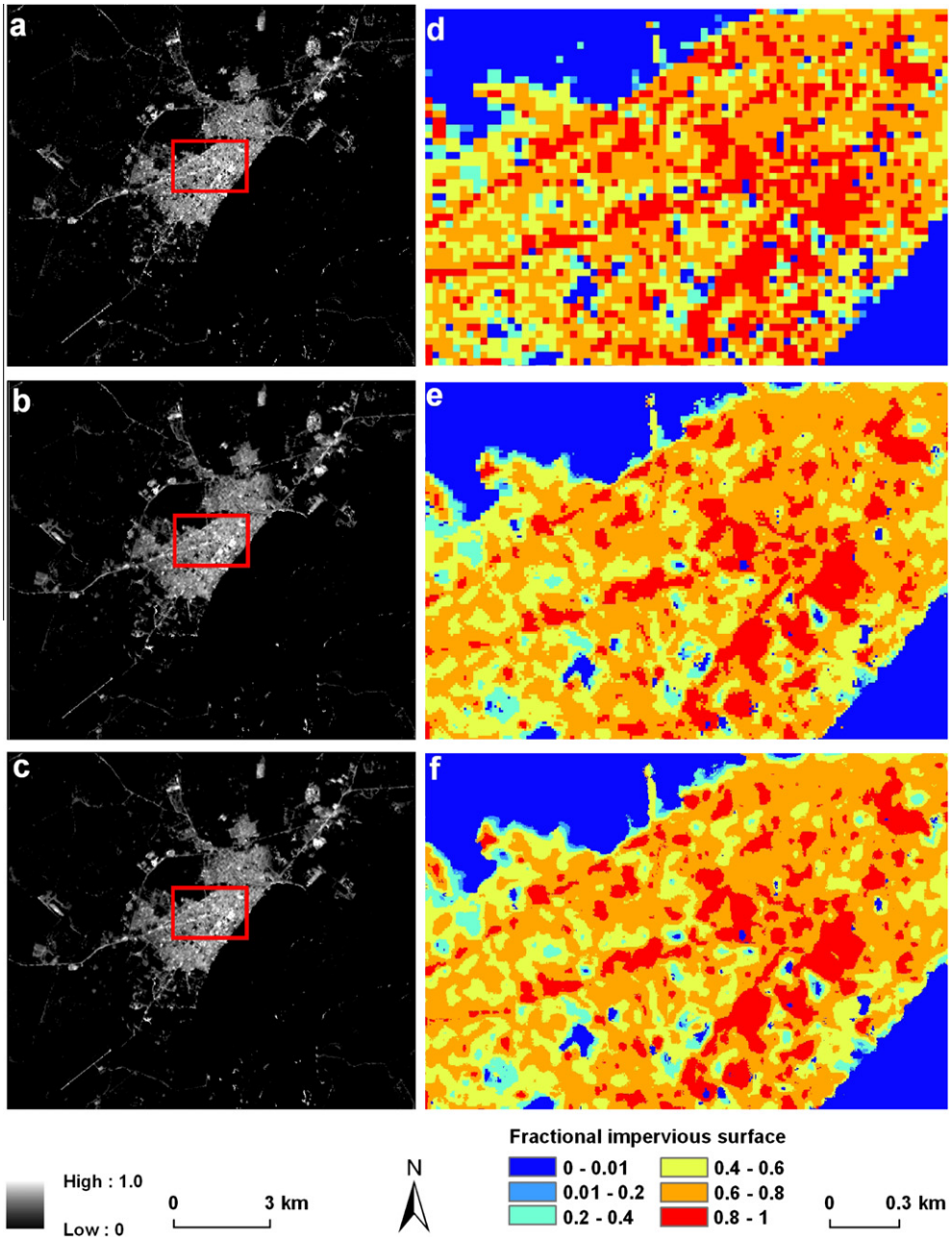

Fig. 7. Comparison of impervious surface spatial patterns (a, b, c are impervious surface images developed from Landsat TM multispectral data with 30 m, from data fusion images of TM and RADARSAT-2 C-band HH data with 10 m and 3 m respectively; d, e, and f are color images with six categories corresponding to a, b and c).

fraction images with 3 m pixel spacing, implying the potential to improve the impervious surface mapping performance in the higher spatial resolution image.

A comparison of extracted impervious surface images among different datasets (Fig. 6) indicates that the data fusion images based on TM multispectral and either PALSAR L-band data with 10 m spatial resolution or RADARSAT C-band data with 10 m or 3 m spatial resolution produced similar impervious surface spatial patterns. However, the impervious surface images generated from either the TM multispectral data image or the fusion image based on TM and RADARSAT-2 C-band HH data with 30-m spatial resolution appear fuzzy, implying their mixed pixel problem due to the coarse spatial resolution in the complex urban–rural landscape. The results in Fig. 6 imply that different wavelengths (L-band or C-band) did not have significantly different roles in impervious surface mapping when they were used in data fusion with the wavelet-based method, but the different spatial resolutions in radar data played an important role in improving the impervious surface distribution patterns. Fig. 7 further confirms the improved spatial patterns from the increased spatial resolution (10 m and 3 m here) compared to the result based on the 30-m TM image. This result implies that impervious surface mapping requires remote-sensing data with better than 10-m spatial resolution. The Landsat TM image with 30-m spatial resolution may be not suitable for impervious surface mapping in a complex urban–rural landscape at local scale.

4.3. Evaluation of impervious surface mapping

A comparison of the relationship between impervious surface data from reference samples and from TM multispectral imagery with 30-m spatial resolution as well as from a fusion image with 3-m spatial resolution shows that higher spatial resolution image provides slightly better performance than lower spatial resolution image, as illustrated in the regression lines and the coefficients of determination (Fig. 8). The residual analysis can more effectively explain which dataset has better results (Fig. 9). When the accuracy assessment was based on single pixels (i.e., 30 × 30 m), it was obvious that impervious surfaces were more prone to be overestimated (Fig. 9: upper) if the proportion of impervious surfaces in a pixel (30 × 30 m) was less than 0.5, but impervious surfaces became underestimated if the proportion was great than 0.5, especially greater than 0.85. This situation is similar to our previous research in impervious surface mapping with Landsat images (Lu and Weng, 2006; Lu et al., 2011b). Meanwhile, as shown in Fig. 9, the residuals from TM with 30-m spatial resolution were obviously higher than those from fusion images with 10-m and 3-m spatial resolutions, and the residuals from the fusion images with 10-m and 3-m spatial resolutions were similar. This result implies the importance of selecting images with suitable spatial resolution for impervious surface mapping. The 30-m spatial resolution Landsat TM image may be too coarse for impervious surface mapping in urban–rural landscapes, because of the spatial patterns were poor and residuals were high compared to the fusion images with 10-m or higher spatial resolution. The multispectral image with 10-m spatial resolution is suitable for impervious surface mapping; however, higher spatial resolution images may not be necessary because the accuracy and spatial patterns are not significantly improved. When the accuracy assessment was based on a window size of 3 × 3 pixels (i.e., 90 × 90 m), the conclusion about which resolution image had mapped better was the same as from a

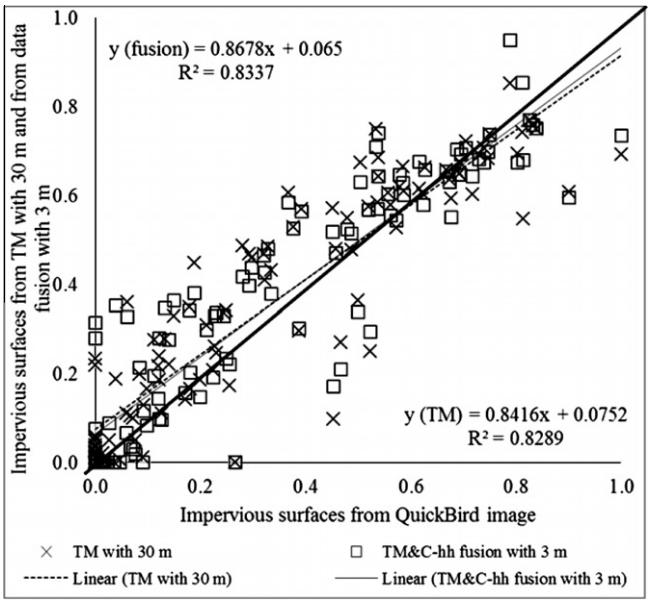

Fig. 8. Comparison of relationship between impervious surface samples from QuickBird and from Landsat image with 30 m as well as from fusion image with 3 m spatial resolution.

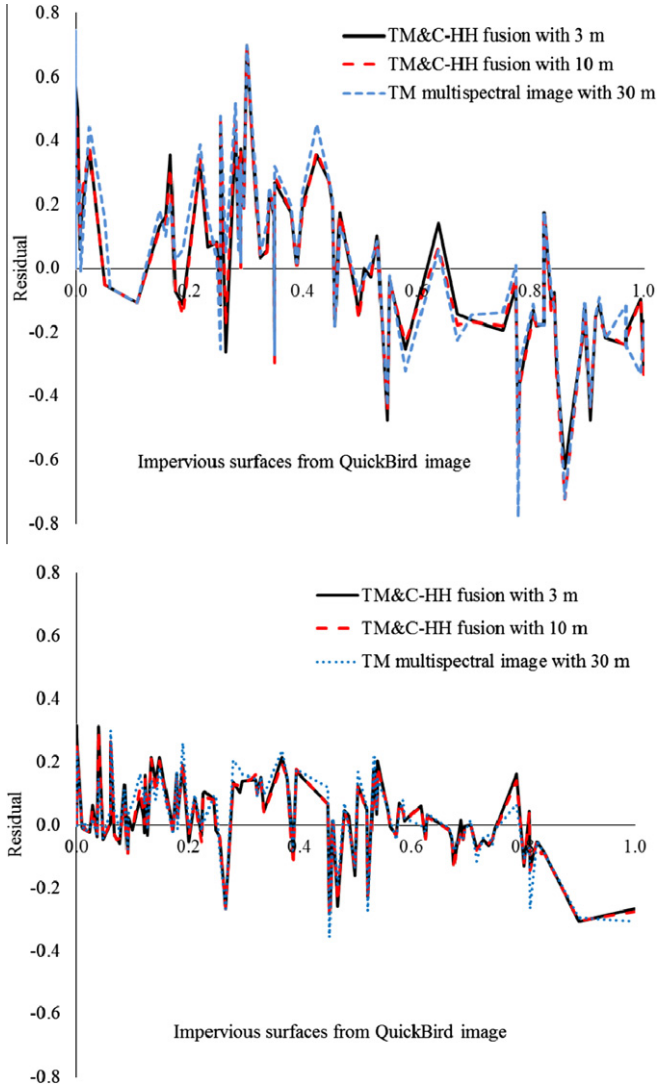

Fig. 9. Residual analysis of impervious surface results (Upper: based on single pixels; Lower: based on a window size of 3 by 3 pixels).

Table 2
Comparison of root mean square errors (RMSE) and correlation coefficients (R) among different scenarios based on single pixel and on a window size of 3 by 3 pixels.

Datasets	RMSE		R	
	Single pixel	3 × 3 pixels	Single pixel	3 × 3 pixels
TM image with 30 m	0.2816	0.1224	0.63	0.91
TM&C-band fusion with 30 m	0.2947	0.1367	0.60	0.89
TM&L-band fusion with 10 m	0.2589	0.1164	0.67	0.92
TM&C-band fusion with 10 m	0.2667	0.1152	0.66	0.92
TM&C-band fusion with 3 m	0.2628	0.1198	0.67	0.91

single pixel; however, the residuals were obviously reduced (Fig. 9: lower) compared to the residuals based on single pixels (Fig. 9: upper). This situation implies the scale issue in how to conduct the accuracy assessment, especially for the fractional images, for which no universal standards are available.

The RMSE and correlation analysis (Table 2) indicates that if accuracy assessment is based on an individual pixel in TM images (i.e., 30 × 30 m), the impervious surface result from data fusion of TM and PALSAR L-band data with 10-m spatial resolution provides the best accuracy (lowest RMSE and highest correlation coefficient), followed by data fusion with RADARSAT-2 C-band with 3-m and 10-m spatial resolution, but the difference in their RMSE values is very small, only 0.0078. Considering the geometric errors between reference data and the impervious surface images, a window size of 3 × 3 pixels (i.e., 90 × 90 m based on the TM image) is often used. The RMSE results indicate that the data fusion images with 10 m or 3 m are similar, with RMSE values of less than 0.12 and correlation coefficient of greater than 0.91, but the data fusion with 30 m had the poorest performance. Both residual analysis and RMSE results imply the important role of radar data with higher spatial resolution in improving impervious surface estimation, especially for spatial patterns. Table 2 also shows that using similar spatial resolution radar data for data fusion with a Landsat TM image cannot improve impervious surface mapping, or the RMSE and spatial patterns. This research implies that use of higher spatial resolution radar data mainly improved the spatial patterns by reducing the mixed pixel problem, but did not significantly improve the spectral features between impervious surfaces and other land covers. In summary, this research indicates that multispectral images with spatial resolution of better than 10 m are suitable for impervious surface mapping, even in a relatively complex urban–rural landscape. High spatial resolution radar data play an important role in improving spatial patterns while preserving multispectral features. The correlation analysis has obtained a similar conclusion as RMSE and residual analysis.

5. Conclusion

Impervious surface mapping with Landsat TM imagery is a challenge, especially in a complex urban–rural landscape due to the mixed pixel problem and similar spectral signatures between impervious surfaces and other land covers such as bare soil and water. This research shows the importance of improved spatial resolution of remotely sensed data by using data fusion of TM multispectral and radar data with higher spatial resolution for improving the impervious surface mapping performance. If the concern is in the statistical area, Landsat TM image can provide accuracy similar to that of higher spatial resolution but with relatively poor spatial patterns. When the concern is in the accurate spatial patterns of impervious surface distribution, selection of higher spatial resolution images for impervious surface mapping is necessary, and the fusion of TM and radar data is an alternative. This research also implies that multispectral images with 30-m spatial resolution is too coarse for impervious surface mapping in the urban–rural landscapes, but the multispectral images with 10-m spatial resolution are suitable, providing similar results as higher spatial resolution images such as 3 m in this research. This research indicated that higher spatial resolution radar data played an important role in improving impervious surface mapping performance, but different wavelengths of radar data (e.g., L-band and C-band data in this research) did not provide significantly different results, implying the role of radar data is in reducing the mixed pixel problem, thus improving the spatial patterns of the impervious surface distribution.

Acknowledgments

We wish to thank the National Science Foundation (grant #BCS 0850615) for financial support for this research. C. Freitas would like to thank JAXA (AO 108) for providing the ALOS PALSAR data through its Science Program, and Mateus Batistella thanks the Canadian SOAR Program (#SOAR Project 1957) for the Radarsat-2 data that was used in this research.

References

Adams, J.B., Sabol, D.E., Kapos, V., Filho, R.A., Roberts, D.A., Smith, M.O., Gillespie, A.R., 1995. Classification of multispectral images based on fractions of endmembers: application to land cover change in the Brazilian Amazon. Remote Sensing of Environment 52 (2), 137–154.

Amarsaikhan, D., Blotevogel, H.H., van Genderen, J.L., Ganzorig, M., Gantuya, R., Nergui, B., 2010. Fusing high-resolution SAR and optical imagery for improved urban land cover study and classification. International Journal of Image and Data Fusion 1 (1), 83–97.

Amolins, K., Zhang, Y., Dare, P., 2007. Wavelet based image fusion techniques—an introduction, review and comparison. ISPRS Journal of Photogrammetry and Remote Sensing 62 (4), 249–263.

Brabec, E., Schulte, S., Richards, P.L., 2002. Impervious surface and water quality: a review of current literature and its implications for watershed planning. Journal of Planning Literature 16 (4), 499–514.

Chander, G., Markham, B.L., Helder, D.L., 2009. Summary of current radiometric calibration coefficients for Landsat MSS, TM, ETM+, and EO-1 ALI sensors. Remote Sensing of Environment 113 (5), 893–903.

Chavez Jr., P.S., 1996. Image-based atmospheric corrections–revisited and improved. Photogrammetric Engineering & Remote Sensing 62 (9), 1025–1036.

Chen, D., Stow, D.A., 2003. Strategies for integrating information from multiple spatial resolutions into land-use/land-cover classification routines. Photogrammetric Engineering & Remote Sensing 69 (11), 1279–1287.

Congalton, R.G., Green, K., 2008. Assessing the Accuracy of Remotely Sensed Data: Principles and Practices, 2 ed.. CRC Press, Taylor & Francis Group, Boca Raton, FL, pp. 183.

Dai, X., Khorram, S., 1998. A hierarchical methodology framework for multisource data fusion in vegetation classification. International Journal of Remote Sensing 19 (18), 3697–3701.

Dare, P.M., 2005. Shadow analysis in high-resolution satellite imagery of urban areas. Photogrammetric Engineering & Remote Sensing 71 (2), 169–177.

Dong, J., Zhuang, D., Huang, Y., Fu, J., 2009. Advances in multi-sensor data fusion: algorithms and applications. Sensors 9 (10), 7771–7784.

Ehlers, M., Klonus, S., Astrand, P.J., Rosso, P., 2010. Multisensor image fusion for pansharpening in remote sensing. International Journal of Image and Data Fusion 1 (1), 25–45.

ESA (European Space Agency), 2007. Information on ALOS PALSAR products for ADEN users. Technical Note ALOS-GSEG-EOPG-TN-07-0001, Noordwijk, the Netherlands: ESA. http://earth.esa.int/download/alos/PALSAR_info_users_v1.1.pdf (Accessed 20 July, 2011).

Ferreira, L.G., Yoshioka, H., Huete, A., Sano, E.E., 2004. Optical characterization of the Brazilian savanna physiognomies for improved land cover monitoring of the cerrado biome: preliminary assessments from an airborne campaign over an LBA core site. Journal of Arid Environments 56 (3), 425–447.

Gamba, P., Dell'Acqua, F., 2008. Fusion of radar and optical data for identification of human settlements. In: Weng, Q. (Ed.), Remote Sensing of Impervious Surfaces. Taylor & Francis Group, LLC, Boca Raton, FL, pp. 143–159.
Goetz, S.J., Wright, R.K., Smith, A.J., Zinecker, E., Schaub, E., 2003. IKONOS imagery for resource management: tree cover, impervious surfaces, and riparian buffer analyses in the mid-Atlantic region. Remote Sensing of Environment 88 (1–2), 195–208.
Hong, G., Zhang, Y., 2008. Comparison and improvement of wavelet-based image fusion. International Journal of Remote Sensing 29 (3), 673–691.
Jensen, J.R., Cowen, D.C., 1999. Remote sensing of urban/suburban infrastructure and socioeconomic attributes. Photogrammetric Engineering & Remote Sensing 65 (5), 611–622.
Lu, D., Batistella, M., Moran, E., 2007. Land-cover classification in the Brazilian Amazon with the integration of Landsat ETM+ and RADARSAT data. International Journal of Remote Sensing 28 (24), 5447–5459.
Lu, D., Hetrick, S., Moran, E., 2011a. Impervious surface mapping with QuickBird imagery. International Journal of Remote Sensing 32 (9), 2519–2533.
Lu, D., Moran, E., Hetrick, S., 2011b. Detection of impervious surface change with multitemporal Landsat images in an urban-rural frontier. ISPRS Journal of Photogrammetry and Remote Sensing 66 (3), 298–306.
Lu, D., Li, G., Moran, E., Dutra, L., Batistella, M., 2011c. A Comparison of multisensor integration methods for land-cover classification in the Brazilian Amazon. GIScience & Remote Sensing 48 (3), 345–370.
Lu, D., Moran, E., Hetrick, S., Li, G., in press. Mapping impervious surface distribution with the integration of Landsat TM and QuickBird images in a complex urban–rural frontier in Brazil (Chapter 13). Ni-Bin Chang (Ed.), Advances of Environmental Remote Sensing to Monitor Global Changes. CRC Press/Taylor and Francis.
Lu, D., Weng, Q., 2004. Spectral mixture analysis of the urban landscapes in Indianapolis with Landsat ETM+ imagery. Photogrammetric Engineering & Remote Sensing 70 (9), 1053–1062.
Lu, D., Weng, Q., 2006. Use of impervious surface in urban land use classification. Remote Sensing of Environment 102 (1–2), 146–160.
Lucas, R.M., Honzák, M., Curran, P.J., Foody, G.M., Milne, R., Brown, T., Amaral, S., 2000. The regeneration of tropical forests within the Legal Amazon. International Journal of Remote Sensing 21 (15), 2855–2881.
Mallinis, G., Koutsias, N., Tsakiri-Strati, M., Karteris, M., 2008. Object-based classification using Quickbird imagery for delineating forest vegetation polygons in a Mediterranean test site. ISPRS Journal of Photogrammetry and Remote Sensing 63 (2), 237–250.
McNairn, H., Champagne, C., Shang, J., Holmstrom, D., Reichert, G., 2009. Integration of optical and synthetic aperture radar (SAR) imagery for delivering operational annual crop inventories. ISPRS Journal of Photogrammetry and Remote Sensing 64 (5), 434–449.
Moran, E.F., 1975. Pioneer Farmers of the Transamazon Highway: Adaptation and Agricultural Production in Lowland Tropics. Ph.D. Dissertation. University of Florida, Department of Anthropology.
Moran, E.F., 1981. Developing the Amazon. Indiana University Press, Bloomington, Indiana, p.292.
Mustard, J.F., Sunshine, J.M., 1999. Spectral analysis for earth science: investigations using remote sensing data. In: Rencz, A.N. (Ed.), Remote Sensing for the Earth Sciences: Manual of Remote Sensing, third ed. vol. 3. John Wiley & Sons Inc., New York, pp. 251–307.
Pohl, C., van Genderen, J.L., 1998. Multisensor image fusion in remote sensing: concepts, methods, and applications. International Journal of Remote Sensing 19 (5), 823–854.
Powell, R., Roberts, D.A., Hess, L., Dennison, P., 2007. Sub-pixel mapping of urban land cover using multiple endmember spectral mixture analysis: Manaus, Brazil. Remote Sensing of Environment 106 (2), 253–267.
Powell, R.L., Roberts, D.A., 2008. Characterizing variability of the urban physical environment for a suite of cities in Rondonia, Brazil. Earth Interactions 12 (13), 1–32.
Powell, R.L., Roberts, D.A., 2010. Characterizing urban land-cover change in Rondonia, Brazil: 1985–2000. Journal of Latin American Geography 9 (3), 183–211.
Ridd, M.K., 1995. Exploring a V–I–S (Vegetation–Impervious Surface-Soil) model for urban ecosystem analysis through remote sensing: comparative anatomy for cities. International Journal of Remote Sensing 16 (12), 2165–2185.
Roberts, D.A., Numata, I., Holmes, K., Batista, G., Krug, T., Monteiro, A., Powell, B., Chadwick, O.A., 2002. Large area mapping of land-cover change in Rondonia using decision tree classifiers. Journal of Geophysical Research 107 (D20), 8073 LBA 40-1–40-18.
Rosenqvist, A., Shimada, M., Ito, N., Watanabe, M., 2007. ALOS PALSAR: a pathfinder mission for global-scale monitoring of the environment. IEEE Transactions on Geoscience and Remote Sensing 45 (11), 3307–3316.
Sano, E.E., Rosa, R., Brito, J.L.S., Ferreira, L.G., 2010. Land cover mapping of the tropical savanna region in Brazil. Environmental Monitoring and Assessment 166 (1–4), 113–124.
Slonecker, E.T., Jennings, D., Garofalo, D., 2001. Remote sensing of impervious surface. a review. Remote Sensing Reviews 20 (3), 227–255.
Smith, M.O., Ustin, S.L., Adams, J.B., Gillespie, A.R., 1990. Vegetation in deserts: I. a regional measure of abundance from multispectral images. Remote Sensing of Environment 31 (1), 1–26.
Smith, N., 1982. Rainforest Corridors. University of California Press, Berkeley, CA.
Ulfarsson, M.O., Benediktsson, J.A., Sveinsson, J.R., 2003. Data fusion and feature extraction in the wavelet domain. International Journal of Remote Sensing 24 (20), 3933–3945.
Wang, L., Sousa, W.P., Gong, P., Biging, G.S., 2004. Comparison of IKONOS and Quickbird images for mapping mangrove species on the Caribbean coast of Panama. Remote Sensing of Environment 91 (3–4), 432–440.
Weng, Q., Hu, X., Liu, H., 2009. Estimating impervious surfaces using linear spectral mixture analysis with multitemporal ASTER images. International Journal of Remote Sensing 30 (18), 4807–4830.
Wu, C., Murray, A.T., 2003. Estimating impervious surface distribution by spectral mixture analysis. Remote Sensing of Environment 84 (4), 493–505.
Xian, G., Crane, M.P., McMahon, C., 2008. Quantifying multitemporal urban development characteristics in Las Vegas from Landsat and Aster data. Photogrammetric Engineering & Remote Sensing 74 (4), 473–481.
Yang, F., Matsushita, B., Fukushima, T., 2010. A pre-screened and normalized multiple endmember spectral mixture analysis for mapping impervious surface area in Lake Kasumigaura Basin, Japan. ISPRS Journal of Photogrammetry and Remote Sensing 65 (5), 479–490.
Yang, L., Jiang, L., Lin, H., Liao, M., 2009. Quantifying sub-pixel urban impervious surface through fusion of optical and InSAR imagery. GIScience and Remote Sensing 46 (2), 161–171.
Yang, L., Xian, G., Klaver, J.M., Deal, B., 2003. Urban land-cover change detection through sub-pixel imperviousness mapping using remotely sensed data. Photogrammetric Engineering & Remote Sensing 69 (9), 1003–1010.
Zhang, J., 2010. Multisource remote sensing data fusion: status and trends. International Journal of Image and Data Fusion 1 (1), 5–24.
Zhang, Y., 2004. Understanding image fusion. Photogrammetric Engineering & Remote Sensing 70 (6), 657–661.
Zhou, W., Huang, G., Troy, A., Cadenasso, M.L., 2009. Object-based land cover classification of shaded areas in high spatial resolution imagery of urban areas: A comparison study. Remote Sensing of Environment 113 (8), 1769–1777.